HHS Public Access

Author manuscript

Biomed Phys Eng Express. Author manuscript; available in PMC 2023 May 04.

Published in final edited form as:

Biomed Phys Eng Express. ; 8(6): . doi:10.1088/2057-1976/ac9b5c.

Therapeutic effects of *in-vivo* radiodynamic therapy (RDT) for lung cancer treatment: a combination of 15MV photons and 5-aminolevulinic acid (5-ALA)

Dae-Myoung Yang[1,*], **Dusica Cvetkovic**[1], **Lili Chen**[1], **C-M Charlie Ma**[1]

[1]Department of Radiation Oncology, Fox Chase Cancer Center, Philadelphia, PA 19111, USA

Abstract

Objective: Radiodynamic therapy (RDT) uses high-energy photon beams instead of visible/near-infrared light to treat deep-seated tumors that photodynamic therapy cannot achieve due to the low penetration depth of laser beams. The purpose of this study is to investigate the therapeutic effect of RDT with 15 MV photon beams combined with 5-aminolevulinic acid (5-ALA) using a mouse model.

Approach: A subcutaneous C57BL/6 mouse model of KP1 small-cell lung cancer cell line was used. The tumors (N=120) were randomized into four groups to observe individual and synergistic effects of 5-ALA and radiation treatment: control (untreated, N=42), radiation treatment (RT) only (N=20), 5-ALA only (N=20), and RDT (N=38). For the RT only and RDT groups, 4 Gy in a single fraction was delivered to the tumors using 15 MV photons. For the 5-ALA only and RDT groups, 5-ALA was injected at a dose of 100 mg/kg by tail-vein 4 hours prior to RT. The tumor response was assessed by monitoring tumor growth using 1.5T MR, maximum standardized uptake value (SUV_{max}) and total lesion glycolysis (TLG) using [^{18}F]FDG PET/CT, and animal survival.

Main results: RDT achieved a statistically significant delay in tumor growth by 52.1%, 48.1%, and 57.9% 7 days post-treatment compared to 5-ALA only, RT only, and control group ($P<0.001$), respectively. There were no significant differences in tumor growth between 5-ALA only and RT only groups. An additional 38.5–40.9% decrease in tumor growth was observed, showing a synergistic effect with RDT. Furthermore, RDT significantly decreased [^{18}F]FDG uptakes in SUV_{max} and TLG 7 days post-treatment by 47.4% and 66.5% ($P<0.001$), respectively. RDT mice survived the longest of all treatment groups.

Significance: RDT with 15 MV photons and 5-ALA resulted in greater tumor control compared to the control and other treatment groups. A significant synergistic effect was also observed with RDT. These preliminary results demonstrate an effective cancer treatment modality.

Keywords

Radiodynamic therapy (RDT); 5-aminolevulinic acid (5-ALA); Therapeutic effect; Tumor control; Cancer treatment; MRI; PET/CT

[*] DaeMvoung.Yang@fccc.edu .

Ethical Statement

All procedures in studies involving animal experimentations were in accordance with the ethical standards of the Institutional Animal Care and Use Committee and Laboratory Animal Facility of Fox Chase Cancer Center.

Introduction

Radiodynamic therapy (RDT) involves the administration of a photosensitizing agent/photosensitizer, which is activated by high-energy radiation (Hashiguchi *et al* 2002, Nakamura *et al* 2008, Ma *et al* 2014). It has been recently adapted from photodynamic therapy (PDT) by replacing superficial visible or near-infrared light irradiation with penetrating high-energy X-rays with a tolerated dose. 5-aminolevulinic acid (5-ALA) is a commonly used precursor/prodrug that generates a photosensitizer protoporphyrin IX (PpIX) via the heme synthesis pathway (Traylor *et al* 2021). 5-ALA-mediated PDT is a clinically proven treatment modality for several types of cancer: skin, head and neck, and esophageal cancer (Dolmans *et al* 2003, Morgan *et al* 2001, Inoue *et al* 2021). Exogenously administered 5-ALA accumulates within tumor tissue, resulting in about 10–20 times higher PpIX accumulation in tumors rather than in normal tissue (Krieg *et al* 2002, Takahashi *et al* 2019). Accumulated PpIX converts oxygen in surrounding tissues to reactive oxygen species, mainly singlet oxygen species ($^1O_2$), leading to cytotoxicity that kills tumor cells after photoactivation (Ni *et al* 2018, Clement *et al* 2021). Furthermore, adding a substrate/enhancer, such as hydrogen peroxide, promotes the production of $^1O_2$ by supplying extra oxygen into the tissue. It has been shown that PpIX catalyzes the conversion of hydrogen peroxide into $^1O_2$ and further enhances a catalytic activity to produce a higher yield of $^1O_2$ under X-ray irradiation (Zeng *et al* 2015).

PDT has been primarily used for superficial localized tumors because of the limited penetration depth of light. The light intensity decreases exponentially with depth; therefore, PDT is not a suitable treatment modality for large, deep, and systemic tumors. However, high-energy photon radiation (X-rays) used in RDT can overcome the limited penetration depth to activate PpIX. Previous findings have suggested that X-rays can activate PpIX as an energy source instead of light to enhance $^1O_2$ and superoxide radical production (Takahashi and Misawa 2009). Since then, other studies have shown that PpIX activation using X-rays is via indirect activation by way of the Cherenkov light, which is induced by X-rays (Axelsson *et al* 2011, Zhang *et al* 2020). Cherenkov light is emitted when charged particles (such as electrons) pass through a dielectric medium at a speed greater than the phase velocity of light in the medium (Cherenkov 1934). Cherenkov light, induced by high-energy X-ray, has a suitable wavelength to activate PpIX in tissue during RDT. Cherenkov light peaks at 370–430 nm, which coincides with the peak absorption spectrum of PpIX at 380–405 nm (Rimington 1960, Takahashi and Misawa 2009). Furthermore, 6–18 MV radiation, both X-ray photons and electrons, from a clinical linear accelerator can produce Cherenkov light in water and muscle tissue (Axelsson *et al* 2011). A positive correlation has been observed between the emission of Cherenkov light and X-ray energy in water and muscle tissue (Axelsson *et al* 2011, Zhang *et al* 2020).

There has been a concern about the indirect activation of PpIX using Cherenkov light for RDT treatment because the intensity of X-ray induced Cherenkov light is much lower than that of conventional laser light (600–800 nm, from orange/red region of the visible light to infra-red) used in PDT (Axelsson *et al* 2011, Zhang *et al* 2020). However, Cherenkov light may have comparable therapeutic responses to conventional laser light because of

several unique characteristics: 1) soret-band effect – due to the excitation spectra of PpIX, the absorption efficiency of Cherenkov light is much greater than the absorption efficiency of the laser light; for example, the absorption efficiency of 400–405 nm is at least 20–30 times higher than at 630 nm (Zhang *et al* 2020); 2) homogeneous internal activation – the tumor target is irradiated by the external laser light in PDT, which is attenuated by the overlapping tissue; the light intensity falls to about 10% at a depth of 7mm under the skin, which is often the maximum treatment depth for superficial tumors in PDT. Therefore, the light intensity of PDT must be 10–20 times higher than the internally emitted Cherenkov light for treating tumors at the deeper edge of the target volume (Zhang *et al* 2020); 3) coenzyme catalyst – a coenzyme (e.g., carbamide peroxide) can be added as a substrate to photosensitizer PpIX to catalyze more $^1O_2$ with X-ray irradiation (an increase of 2.5–5 times, Zeng *et al* 2015); and 4) the combination of Cherenkov-induced PDT and radiation therapy may provide additional therapeutic benefits for cancer therapy (Ma *et al* 2014). The combined improvements noted above (an increase up to 1000 times) indicate an *equivalent power density* of up to 5 mW/cm^2 for RDT, which is within the range of 1 – 10^2 mW/cm^2 for conventional PDT using the 630nm laser light (Zhang *et al* 2020).

Several groups have studied the effectiveness of 5-ALA-mediated RDT *in-vitro* and *in-vivo* in immunocompromised or immunocompetent mice using a kV X-ray irradiator; these studies reported the effectiveness of RDT for the brain, colorectal, and prostate model (Kitagawa *et al* 2015, Miyake *et al* 2019, Takahashi *et al* 2013, 2016, 2018, 2019, 2021, Ueta *et al* 2017, Yamada *et al* 2019, Yamamoto *et al* 2012, 2015). Moreover, an effective delay in tumor growth of RDT compared to radiation alone was reported with B16-BL6 melanoma cell line using a low MV (4 MeV) photon beam in immunocompetent mice (Takahashi *et al* 2018). Our group previously investigated the effect of RDT in immunocompromised mice with PC-3 prostate cancer cell line using a high MV (15 MV) photon beam (Panetta *et al* 2020). The results showed that 15 MV irradiation combined with 5-ALA did not improve tumor control compared to radiation alone. However, the addition of intratumoral injection of carbamide peroxide resulted in a significant tumor growth delay for the tumor model investigated. The potential of using hydrogen peroxide has been reported to be an adjuvant to radiodynamic therapy by enhancing cellular radiosensitivity and production of $^1O_2$ (Fang *et al* 2013, Zeng *et al* 2015, Panetta *et al* 2020). Furthermore, 5-ALA also enhanced the host antitumor immune response and thus caused high inhibition of tumor growth in the glioma model (Yamamoto *et al* 2015).

To develop RDT for future clinical applications, we expanded our investigation to other tumor models. In this work, we studied the therapeutic effect of RDT by combining high-energy (15 MV) radiation therapy and 5-ALA administration in an immunocompetent mouse model of lung cancer. The objective of the investigation was to compare the individual and combined effects of the photosensitizer (5-ALA) and high-energy photon (15 MV) on treatment outcomes. The therapeutic effects were assessed using magnetic resonance (MR) imaging, positron emission tomography (PET)/computed tomography (CT) imaging, and the survival of mice.

Method

Lung Cancer Mouse Model

All animal studies were approved by our Institutional Animal Care and Use Committee (IACUC). A subcutaneous murine small-cell lung cancer model in male C57BL/6 mice (Taconic, Rensselaer, NY) was used. Each mouse was implanted subcutaneously with 2×10^6 KP1 cells in 100 μL of Dulbecco's phosphate-buffered saline (PBS) into the bilateral flank (2 inoculated tumors per mouse). Tumor size was monitored daily starting 5 days after implantation. The animals were kept at room temperature, given free access to food and water, and subjected to a 12-hour day/night light schedule.

Experiment Design

When the tumor reached 5–8 mm in diameter, treatment was performed. The tumor-bearing mice were randomized into 4 groups: 1) untreated (control), 2) 5-ALA only, 3) radiation therapy (RT) only, and 4) a combination of 5-ALA and RT (RDT).

Tumor volume was monitored weekly by a 1.5 T MR scanner (GE Healthcare, Waukesha, WI) from the day of treatment for all groups. [^{18}F]FDG uptakes of tumors were measured using an animal *in-vivo* PET/CT scanner (Sofie BioSciences Inc., Culver City, CA) on the day of treatment (prior to treatment, pre-treatment), 3 days post-, 7 days post-, and 10 days post-treatment for the control and RDT groups. Animal survival times were monitored from the day of treatment until death.

External Beam Radiation Therapy

Radiation treatment was performed using 15 MV X-ray beams on a Varian Clinac iX accelerator (Varian Medical Systems, Palo Alto, CA). 15 MV is the highest X-ray energy available on this machine at our institution, which was selected to maximize the emission of Cherenkov light for RDT treatment. 4 Gy in a single fraction was delivered to the tumor target for RT only and RDT groups. Mice were lying in the prone position on the treatment couch with a 3.0 cm bolus (Action Products, Inc. Hagerstown, MD). Radiation fields were collimated to ensure adequate coverage of the tumor volume. Mice were anesthetized with inhalation of 2–3% isoflurane in oxygen. 5-ALA (Cayman Chemicals, Ann Arbor, MI), at a dose of 100 mg/kg, was injected intravenously into the tail-vein 4 hours prior to RT for the 5-ALA only and RDT groups.

Tumor Measurement

Tumor volume was monitored using GE 1.5 T Signa MR scanner (GE Healthcare, Waukesha, WI) weekly on the day of treatment (pre-treatment), 7 days post-, and 14 days post-treatment. A 3-inch surface coil was used to detect the MR signal. T2-weighted (T2w) MR images were acquired using the fast-recovery fast-spin-echo (FRFSE) sequence (TR/TE = 2200/85 ms) with a $0.243 \times 0.243 \times 1.2$ mm^3 resolution (288-by-288 matrix, 7 cm FOV, 1.2 mm slice thickness). The delineation of tumors was done manually. Tumor growth was quantified as the relative change of post-treatment tumor volume at 7 or 14 days to pre-treatment tumor volume.

PET Imaging

In order to investigate the effect of RDT on tumor metabolic activity, the [^{18}F]FDG uptake of the tumor was observed using a PerkinElmer G8 pre-clinical PET/CT scanner (Sofie BioSciences Inc., Culver City, CA) pre-, 3 days post-, 7 days post-, and 10 days post-treatment for the control and RDT groups. A PET scan was acquired with 0.46 × 0.46 × 0.46 mm^3 resolution (Gu *et al* 2019). A cone-beam CT was acquired with 50 kVp, 200 μA, and a resolution of 0.2 × 0.2 × 0.2 mm^3 (Gu *et al* 2019). PET/CT scans were set to cover the whole body. A 10 min static scan was acquired 1 hour after an injection of 80 μCi [^{18}F]FDG. Active metabolic tumor volume by PET was defined by thresholding the standardized uptake value (SUV) > 3 g/mL in the tumor lesions based on the co-registered CT. [^{18}F]FDG PET images were analyzed quantitatively, including assessment of the maximum tumor SUV (SUV_{max}) and total lesion glycolysis in the tumor (TLG). SUV_{max} was calculated as the maximum measured activity concentration divided by the injected dose/body weight. TLG was quantified as a product of SUV_{mean} and the metabolic tumor volume. The metabolic tumor volume is determined as the total number of voxels within the measured PET region of interest (ROI).

Survival of Mice

The survival of mice was calculated using the product-limit Kaplan-Meier estimator. The health of mice was monitored daily by veterinarians and animal technicians in our animal facility. The postmortem (survival) was carried out either at animal death or at euthanasia by CO_2 asphyxiation per established IACUC guidelines. Euthanasia was performed if the tumor burden reached 10% body mass or mice were observed to be in severe pain or distress. Signs of pain and distress included hunched posture, uncontrolled shivering, dehydration, tumor ulceration, weight loss greater than 20%, labored breathing, poor grooming, restricted movements that interfere with daily activity, and lethargy.

Tissue Sampling and Histopathological Images

To qualitatively confirm the correlation between tumor PET signal intensity and histology, an additional 9 mice, 3 for each time point, underwent PET/CT imaging 3-, 7-, and 10-days post-treatment. These mice were not included in the principal analysis (tumor growth, [^{18}F]FDG uptake, and survival). After PET/CT scan, the mice were euthanized via CO_2 asphyxiation. Tumor specimens were harvested, fixed in 10% neutral buffered formalin, embedded in paraffin, cut into 4 μm serial sections, and stained with hematoxylin & eosin (H&E). To assess the morphology of the tumors and to quantitate the necrosis area, the H&E slides were scanned using the Scanscope XT (Aperio Technologies Inc., Vista, CA). For each tumor, the total tumor area, as well as areas of necrosis within the tumor, were selected and measured using the ImageScope Software (Aperio Technologies Inc., Vista, CA).

Statistical Analysis

All statistical analyses were performed using IBM SPSS Statistics 27 (IBM Corp., Armonk, NY) with two-sided statistical testing with significance accepted at $P<0.05$. Two-way repeated ANOVA with Bonferroni correction was used to compare each treatment group to determine the statistically significant difference in tumor growth, SUV_{max}, and TLG.

A Pearson correlation was used to determine the relationship between two volumes measured in MR and [^{18}F]FDG PET/CT. A Spearman correlation was used to determine the relationship between the number of metastasis, tumor volume, SUV_{max}, and TLG. A Kaplan-Meier survival analysis was conducted to compare the four different treatment groups.

Results

A total of 120 tumors (60 mice, 2 inoculated tumors per mouse) were analyzed in this study. The tumors were assigned into four groups: control (N=42), RT only (N=20), 5-ALA only (N=20), and RDT group (N=38). They were investigated to observe the therapeutic effect of RDT using MR imaging, PET/CT imaging, and survival of mice.

Tumor Growth

RDT resulted in a statistically significant decrease in tumor growth compared to 5-ALA only ($P<0.001$), RT only ($P<0.001$), and the control group ($P<0.001$). Figure 1 shows the tumor growth (relative change in tumor volume) based on the experimental results. The untreated control group had continuous tumor growth. The RT only group suppressed the mean tumor growth by 22.5 ± 10.2% and 20.7 ± 9.2% at 7 days and 14 days post-treatment, respectively. The 5-ALA only group suppressed the mean tumor growth by 16.0 ± 11.5% and 11.8 ± 9.6% at 7 days and 14 days post-treatment, respectively. However, the tumor growth of RT only and 5-ALA only did not show a statistically significant difference. Most importantly, the RDT group had a significant tumor growth delay compared to 5-ALA only, RT only, and the control group by 52.1 ± 11.7%, 48.1 ± 9.8%, and 57.9 ± 13.0% at 7 days post-treatment and 49.0 ± 14.6%, 43.3 ± 14.7%, and 53.0 ± 17.2% at 14 days post-treatment, respectively. Moreover, additional 38.5–40.1% decrease in tumor growth was observed as a synergistic effect of combining 15 MV radiation and 5-ALA, based on the MR measured volume of RT only, 5-ALA only, and RDT groups. Figure 2 shows T2w MR images in each group at pre-, 7 days post-, and 14 days post-treatment.

Tumor Activity

The RDT group showed a significant reduction in SUV_{max} ($P<0.001$) and TLG ($P<0.001$) compared to the control group. SUV_{max} showed 36.9 ± 5.6%, 47.4 ± 8.8%, and 28.7 ± 5.7% decrease at 3-, 7-, and 10-days post-treatment, respectively. TLG showed 56.9 ± 3.1%, 66.5 ± 5.3%, and 54.2 ± 4.1% decrease at 3-, 7-, 10-days post-treatment, respectively. Figure 3 shows the relative change in SUV_{max}, and TLG to the pre-treatment, and figure 4 shows a 3D whole-body [^{18}F]FDG PET scan of a mouse in each group at 7 days post-treatment. From Figure 4, we can observe that the tumors in the control group have higher [^{18}F]FDG uptake than the tumors in the RDT group. Also, there are more mice with multiple distant metastases developed in the control group than in the RDT group (Table 1). A total of 9 mice in the control group and 4 in the RDT group showed metastases using [^{18}F]FDG PET/CT within 10 days post-treatment. Table 1 shows the total number of metastases observed in mice with [^{18}F]FDG PET/CT in the control and the RDT group. The total number of metastases showed a statistically significant positive correlation with tumor growth (R^2=0.99, P<0.01), TLG (R^2=0.99, P<0.01), and SUV_{max} (R^2=0.66, P<0.05).

In addition, tumor necrotic cores were observed by comparing tumor volumes measured by MR and PET/CT imaging. A mismatch between two volumes indicated a necrotic core in the tumor. The necrotic cores were validated using histopathological images. Volumes measured by PET and MR had a correlation of R^2=0.77 ($P<0.001$). Figure 5 shows the scatter plot of tumor volumes measured in MR and PET/CT and an example of an axial PET image superimposed on the CT image with corresponding histopathological slides.

Survival

Mice that underwent RDT survived for or were euthanized after an average of 28.9 ± 1.8 days. This period of time was significantly longer than for the groups receiving RT only, 5-ALA only, or the control group, which had a mean survival time of 22.9 ± 2.0 days ($P<0.05$), 24.3 ± 1.6 days ($P<0.05$), and 21.5 ± 1.2 days ($P<0.01$), respectively. The other three groups had no significant difference in survival time between each other. Figure 6 shows the overall survival curve of each group.

Discussion

In this study, we investigated the therapeutic effect of RDT treatment with a combination of 15 MV radiation and 5-ALA on a murine lung tumor model *in vivo*.

Our MR tumor growth measurements showed a significant improvement in tumor control with RDT compared to RT and 5-ALA alone. These results are consistent with previous studies using glioblastoma cell lines in nude mice (Takahashi *et al* 2021). U251MG and U87MG glioblastoma cell lines in nude mice showed tumor regression with a multi-fractionated RT scheme (total dose of 60 Gy, 2 Gy/fraction) using a ^{137}Cs irradiator and 60–120 mg/kg of 5-ALA (Takahashi *et al* 2021). However, our previous study with PC-3 prostate cancer cell line in nude mice only showed small tumor growth delay using 15 MV RT and 5-ALA (within experimental uncertainties); the treatment effects on the PC-3 cell line in nude mice were improved significantly by adding carbamide peroxide, which resulted in a higher yield of the $^1O_2$ by PpIX catalytic activity under X-ray irradiation (Panetta *et al* 2020). Many factors may affect the treatment outcomes between our previous and current studies, e.g., mouse model, tumor cell line, radio-sensitivity, tumor biochemical environment, etc. A nude mouse is an immune-compromised mouse strain and PC-3 is an aggressive, radiation-resistant prostate tumor cell line. Thus, the reduced tumor growth delay observed in our previous experiments may be explained by the lack of radiation- and Cherenkov light PDT-induced anti-cancer immune responses and radio-resistance. The C57BL/6 mouse in this work is a regular immunocompetent black mouse strain, and the small-cell lung cancer KP1 cells responded well to RDT. Favorable RDT responses were also obtained with a B16-BL6 mouse melanoma model (Takahashi *et al* 2018), who irradiated the tumors using either 160 kV X-rays or 4 MeV photon beams (20–30 Gy) after 5-ALA administration (50 mg/kg). Their gene expression profiles and tumor suppression results demonstrated that 5-ALA works as a radiosensitizer with X-ray irradiation at both kilovoltage and megavoltage energies (Takahashi *et al* 2018).

The results of our current study demonstrated a synergistic effect of 15 MV radiation and 5-ALA. This synergistic effect, based on the tumor growth delay, suggests that there is a

benefit of combining high-energy 15 MV radiation with 5-ALA in the treatment, which is consistent with the analyses of Zhang *et al* (2020). In fact, some mice in the RDT group showed a decrease in tumor volume 7 days post-treatment, as shown in Figure 2. The results obtained with MR images alone lend support to the use of high-energy radiation in RDT. When we compared the individual vs. synergistic effect of RDT, the major difference between the two is the PpIX activation via Cherenkov light. Therefore, the evidence suggests that PpIX activation caused by the Cherenkov light can be estimated using the synergistic effect of 15 MV radiation and 5-ALA. If the suggestion holds, a higher radiation energy can produce a greater synergistic effect due to more emission of Cherenkov light.

Tumor activity measured by [^{18}F]FDG PET/CT consolidates the previous MR results. The therapeutic response was evaluated by TLG and SUV_{max} using [^{18}F]FDG PET/CT. Since there were no significant differences in tumor growth with the 5-ALA only and RT only compared with control groups on MR, evaluation of the [^{18}F]FDG/CT was performed only for the control and RDT groups due to animal ethics and high cost of [^{18}F]FDG. TLG reflects the functional glucose uptake within the metabolic volume by combining volumetric and metabolic information of FDG (Chen *et al* 2012). SUV_{max} reflects tumor maximum glucose uptake. RDT resulted in a significant reduction, compared to the control group, in both TLG and SUV_{max}, indicating that RDT suppressed tumor activity. Relative changes in SUV_{max} exhibited a plateau 3 days after treatment (figure 3B), but not in TLG (figure 3A). Results suggest that TLG may be a more suitable parameter than SUV_{max} to observe the progression of tumor response after treatment. Additionally, a total number of metastases observed by [^{18}F]FDG PET/CT imaging showed an excellent correlation between tumor growth and TLG, which is in agreement with other studies (Shan *et al* 2019, Kang *et al* 2020). The primary tumor volume showed a positive correlation with the circulating tumor cells (Kang *et al* 2020). As tumors get bigger, they release circulating tumor cells into peripheral blood circulation, leading to metastatic spread.

A mismatch between MR and PET/CT volumes indicated a necrotic core in the tumor. Digital histopathological images validated that the hypo-intensity signal in the middle of the tumor on [^{18}F]FDG PET/CT was indeed the necrotic core (figure 5B, D–E). When the tumor is small, active (proliferating) tumor cells occupy the majority of the tumor volume; therefore, the bias of the volume measured with [^{18}F]FDG PET is insignificant (figure 5A). However, the larger the tumor, the greater the bias because the center of the tumor is filled with necrotic dead cells.

The RDT group had a mean survival of 28.3 ± 1.9 days, about 7 days longer than the control group (21.6 ± 2.2 days). This finding supports our tumor growth delay results. The relative tumor volume change also showed that RDT treatment delayed the tumor growth by about 7 days compared to the control group. The RDT group at 14 days post-treatment had a tumor growth of 3.36 ± 0.52, and the control group at 7 days post-treatment had a tumor growth of 3.45 ± 0.34 (figure 1).

This study delivered the radiation to the mouse lung tumor in a single fraction of 4 Gy, along with a 5-ALA injection, to determine the tumor cell-killing effect. It showed significant improvement compared to untreated, radiation treatment only, and 5-ALA only groups.

Furthermore, RDT was reported with no severe toxicity to the healthy tissues (Takahashi *et al* 2021), and its effect improved with the addition of carbamide peroxide to the treatment protocol to generate extra reactive oxygen species (Panetta *et al* 2020). These results suggest that RDT is effective in tumor control and support a comprehensive analysis of treatment outcomes as a function of the 5-ALA dose, radiation energy, dose and fractionation.

Conclusion

Assessment of radiodynamic therapy combined with 5-ALA administration and 15 MV high-energy radiation treatment showed improved treatment outcomes compared to the control, radiation therapy only, and 5-ALA only groups. Tumor growth delay, tumor activity suppression, and survival were significantly improved with RDT. Moreover, a synergistic effect of 5-ALA and 15 MV X-rays was observed. The preliminary results demonstrate a potential of RDT for cancer therapy.

Acknowledgments

This publication was supported by Grant No. P30 CA006927 from the National Cancer Institute, NIH. Its contents are solely the responsibility of the authors and do not necessarily represent the official views of the National Cancer Institute or the National Institutes of Health. We would like to thank the core research facilities at Fox Chase Cancer Center for their technical support.

References

Axelsson J et al. 2011 Cerenkov emission induced by external beam radiation stimulates molecular fluorescence Medical physics 38(7) 4127–4132 [PubMed: 21859013]

Chen HHW et al. 2012 Prognostic value of whole-body total lesion glycolysis at pretreatment FDG PET/CT in non–small cell lung cancer Radiology 264(2) 559–566 [PubMed: 22692034]

Cherenkov PA 1934 Visible light from clear liquids under the action of gamma radiation Comptes Rendus (Doklady) de I'Aeademie des Sciences de I'URSS 2(8) 451–4.

Clement S et al. 2021 Oxygen-Carrying Polymer Nanoconstructs for Radiodynamic Therapy of Deep Hypoxic Malignant Tumors Biomedicines 9(3) 322 [PubMed: 33810115]

Dolmans DEJGJ, Fukumura D and Jain RK 2003 Photodynamic therapy for cancer Nature reviews cancer 3(5) 380–387 [PubMed: 12724736]

Fang Y et al. 2013 Hydrogen Peroxide Enhances Radiation-induced Apoptosis and Inhibition of Melanoma Cell Proliferation Anticancer Research 33(5) 1799–807 [PubMed: 23645724]

Gu Z et al. 2019 Performance evaluation of G8, a high-sensitivity benchtop preclinical PET/CT tomograph Journal of Nuclear Medicine 60(1) 142–149 [PubMed: 29903933]

Hashiguchi S et al. 2002 Acridine orange excited by low-dose radiation has a strong cytocidal effect on mouse osteosarcoma Oncology 62(1) 85–93 [PubMed: 11810048]

Inoue T and Ishihara R 2021 Photodynamic therapy for esophageal cancer Clinical Endoscopy 54(4) 494 [PubMed: 32422695]

Kang BJ et al. 2020 Circulating tumor cell number is associated with primary tumor volume in patients with lung adenocarcinoma Tuberculosis and respiratory diseases 83(1) 61–70 [PubMed: 31905433]

Kitagawa T et al. 2015 5-Aminolevulinic acid strongly enhances delayed intracellular production of reactive oxygen species (ROS) generated by ionizing irradiation: Quantitative analyses and visualization of intracellular ROS production in glioma cells in vitro Oncology Reports 33(2) 583–90 [PubMed: 25420428]

Krieg RC et al. 2002 Metabolic Characterization of Tumor Cell–specific Protoporphyrin IX Accumulation After Exposure to 5-Aminolevulinic Acid in Human Colonic Cells Photochemistry and Photobiology 76(5) 518–25. [PubMed: 12462647]

Ma CM et al. 2014 Radio-Dynamic Therapy (RDT) for the Treatment of Late-Stage Cancers Medical Physics 41(6) 312–313

Miyake M et al. 2019 Dual benefit of supplementary oral 5-aminolevulinic acid to pelvic radiotherapy in a syngenic prostate cancer model Prostate 79(4) 340–351 [PubMed: 30450646]

Morgan J and Oseroff AR 2001 Mitochondria-based photodynamic anti-cancer therapy Advanced drug delivery reviews 49(1–2) 71–86 [PubMed: 11377804]

Nakamura T et al. 2008 A new limb salvage surgery in cases of high-grade soft tissue sarcoma using photodynamic surgery, followed by photo- and radiodynamic therapy with acridine orange Journal of surgical oncology 97(6) 523–528. [PubMed: 18348188]

Ni K et al. 2018 Nanoscale metal-organic frameworks for mitochondria-targeted radiotherapy-radiodynamic therapy Nature communications 9(1) 1–13

Panetta JV et al. 2020 Radiodynamic therapy using 15-MV radiation combined with 5-aminolevulinic acid and carbamide peroxide for prostate cancer in vivo Physics in Medicine & Biology 65(16) 165008 [PubMed: 32464613]

Rimington C 1960 Spectral-absorption coefficients of some porphyrins in the Soret-band region Biochemical Journal 75(3) 620 [PubMed: 16748818]

Shan Q et al. 2019 Relationship between tumor size and metastatic site in patients with stage IV non-small cell lung cancer: a large SEER-based study PeerJ 7 e7822 [PubMed: 31616594]

Takahashi J and Misawa M 2009 Characterization of reactive oxygen species generated by protoporphyrin IX under X-ray irradiation Radiation Physics and Chemistry 78(11) 889–898

Takahashi J et al. 2013 5-Aminolevulinic acid enhances cancer radiotherapy in a mouse tumor model Springerplus 2(1) 602 [PubMed: 24324921]

Takahashi J et al. 2016 Combined treatment with X-ray irradiation and 5-aminolevulinic acid elicits better transcriptomic response of cell cycle-related factors than X-ray irradiation alone International Journal of Radiation Biology 92(12) 774–789 [PubMed: 27586078]

Takahashi J et al. 2018 Verification of radiodynamic therapy by medical linear accelerator using a mouse melanoma tumor model Scientific Reports 2018 8(1) 1–9 [PubMed: 29311619]

Takahashi J et al. 2019 Verification of 5-aminolevurinic Radiodynamic therapy using a murine melanoma brain metastasis model International Journal of Molecular Sciences 20(20) 5155 [PubMed: 31627442]

Takahashi J et al. 2021 In Vivo Study of the Efficacy and Safety of 5-Aminolevulinic Radiodynamic Therapy for Glioblastoma Fractionated Radiotherapy International Journal of Molecular Sciences 22(18) 9762 [PubMed: 34575921]

Traylor JI et al. 2021 Molecular and Metabolic Mechanisms Underlying Selective 5-Aminolevulinic Acid-Induced Fluorescence in Gliomas Cancers 13(3) 580 [PubMed: 33540759]

Ueta K et al. 2017 5-Aminolevulinic acid enhances mitochondrial stress upon ionizing irradiation exposure and increases delayed production of reactive oxygen species and cell death in glioma cells International Journal of Molecular Medicine 39(2) 387–398 [PubMed: 28035368]

Yamada K et al. 2019 Radiosensitizing effect of 5-aminolevulinic acid in colorectal cancer in vitro and in vivo Oncology Letters 17(6) 5132–5138 [PubMed: 31186727]

Yamamoto J et al. 2012 Radiosensitizing effect of 5-aminolevulinic acid-induced protoporphyrin IX in glioma cells in vitro Oncology reports 27(6) 1748–52 [PubMed: 22378066]

Yamamoto J et al. 2015 5-aminolevulinic acid-induced protoporphyrin IX with multi-dose ionizing irradiation enhances host antitumor response and strongly inhibits tumor growth in experimental glioma in vivo Molecular medicine reports 11(3) 1813–9. [PubMed: 25420581]

Zeng J et al. 2015 Protoporphyrin IX catalyzed hydrogen peroxide to generate singlet oxygen International Journal of Clinical and Experimental Medicine 8(5) 6829–6834 [PubMed: 26221221]

Zhang Q et al. 2020 Investigation of the Mechanisms of Radio-Dynamic Therapy Mathews Journal of Cancer Science 5(1) 1–9

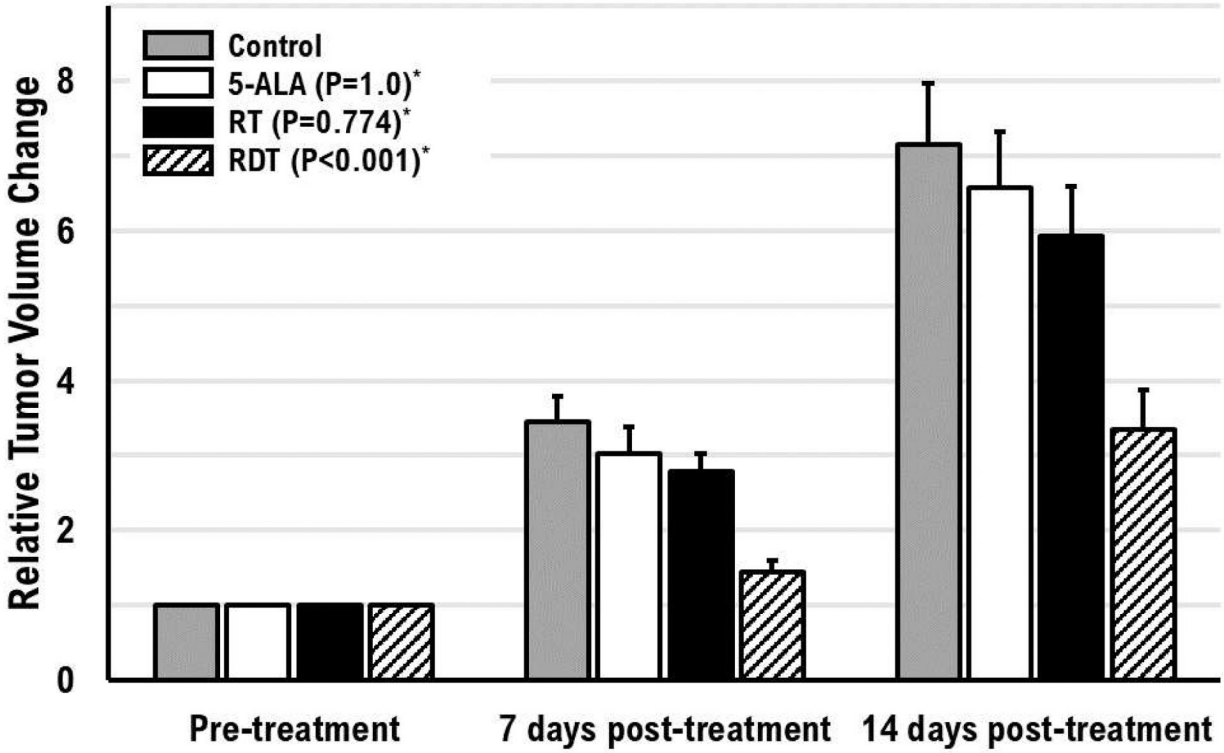

Figure 1.

Tumor growth (relative tumor volume change from post-treatment tumor volume to pre-treatment tumor volume) after single-fraction treatment of RT, 5-ALA, or RDT (combination of RT and 5-ALA) for 14 days. The error bars are the standard deviation of the mean. (*Compared to the control group)

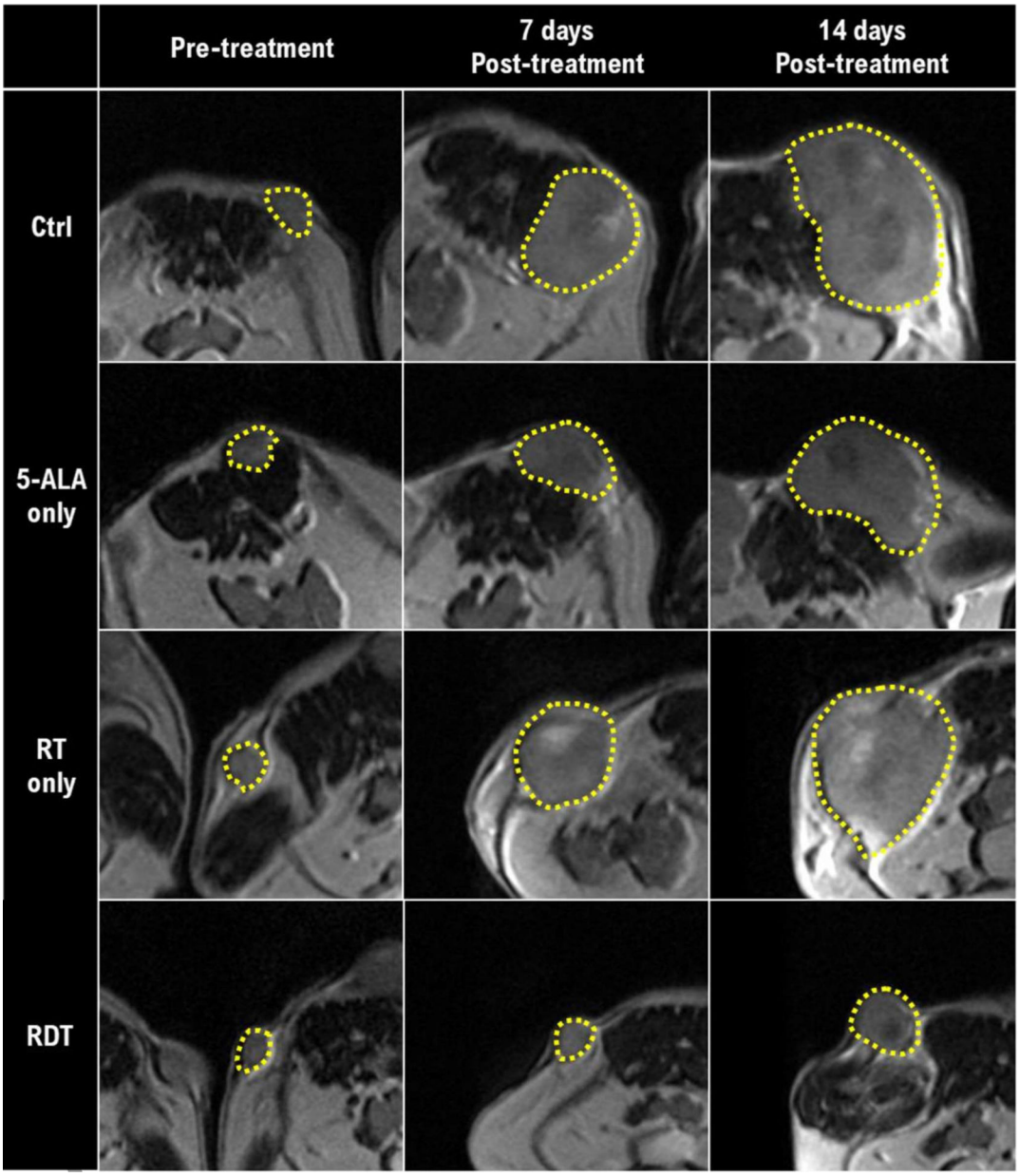

Figure 2.
Axial T2-weighted mouse MR images. The yellow dotted lines indicate the tumor delineation of each mouse. Rows represent treatment groups, and columns represent time points.

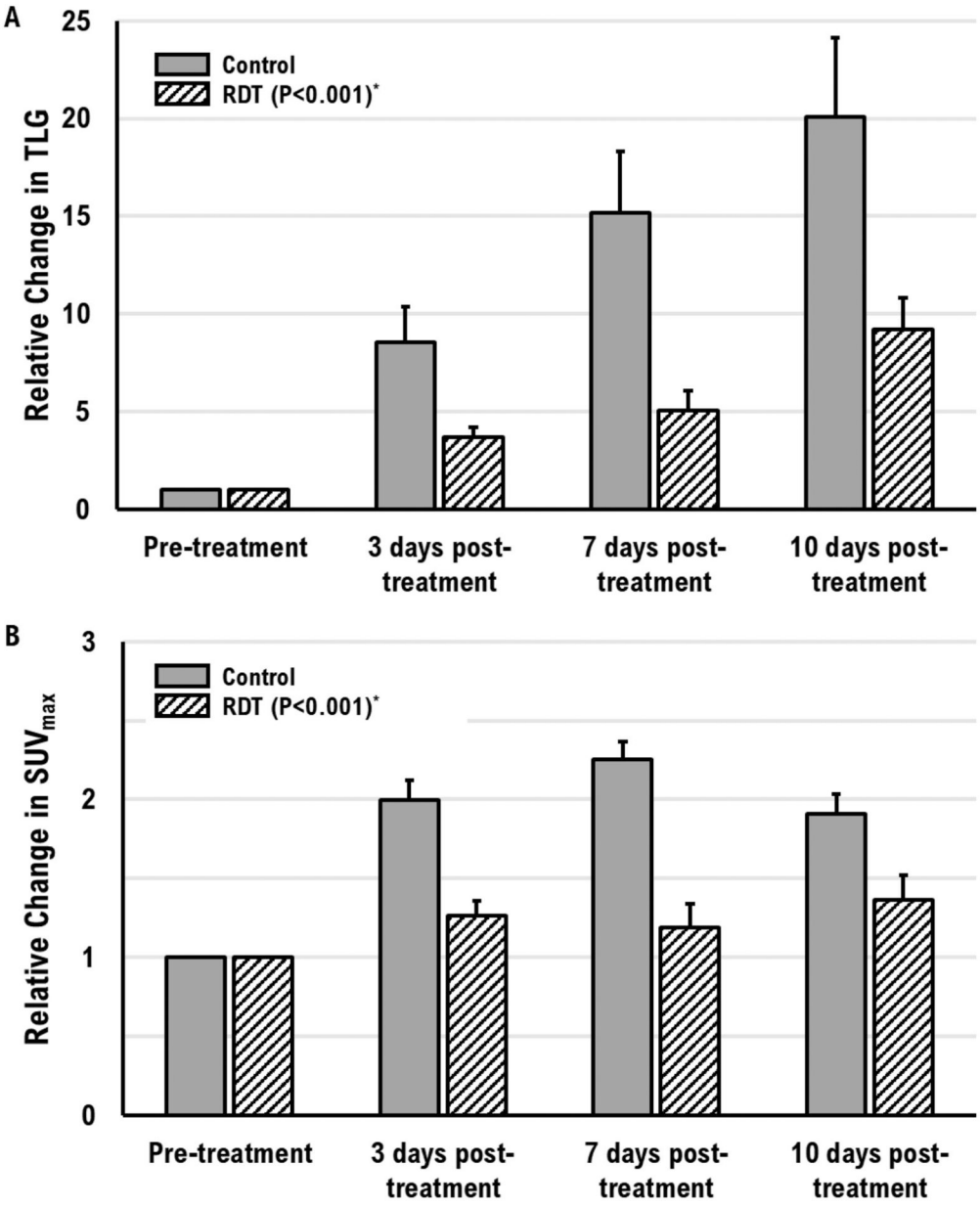

Figure 3.

Relative change in (A) TLG and (B) maximum SUV from post-treatment to pre-treatment. The error bars are the standard deviation of the mean. (*Compared to the control group)

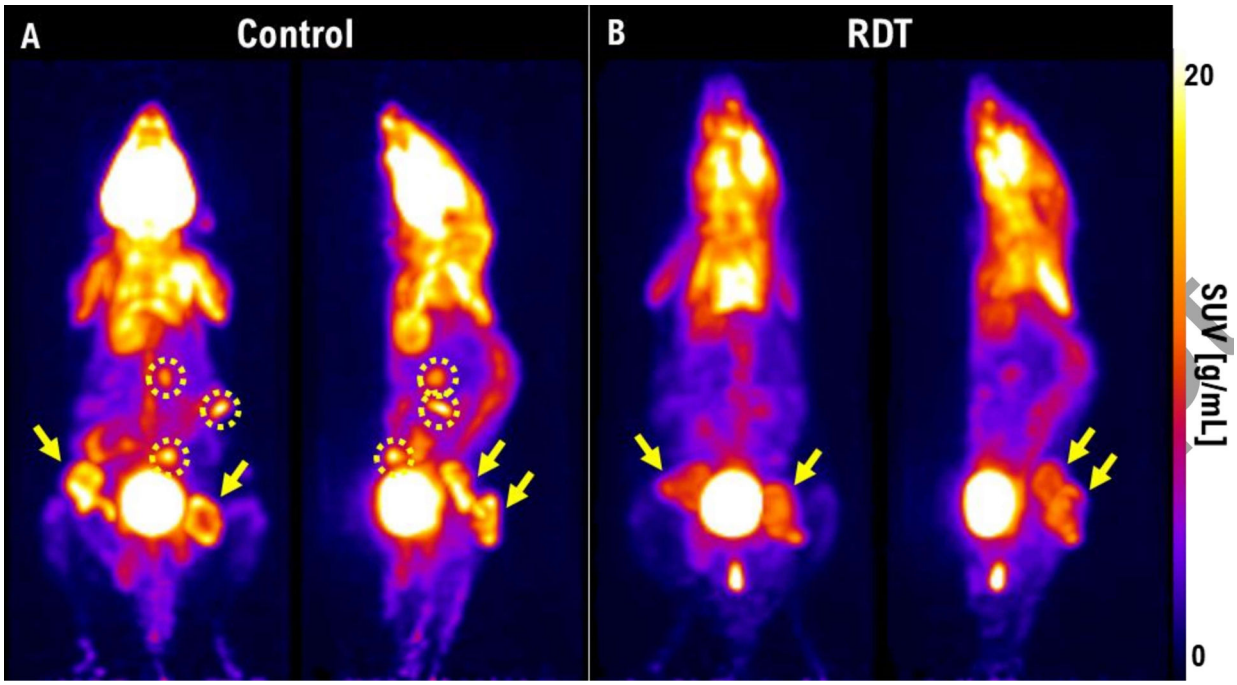

Figure 4.

A 3D whole-body [^{18}F]FDG PET scans of a mouse in (A) control and (B) RDT group at 7 days post-treatment. The yellow arrows indicate the primary tumor sites in the bilateral flanks of the mice. The yellow dotted circles indicate the metastasis sites.

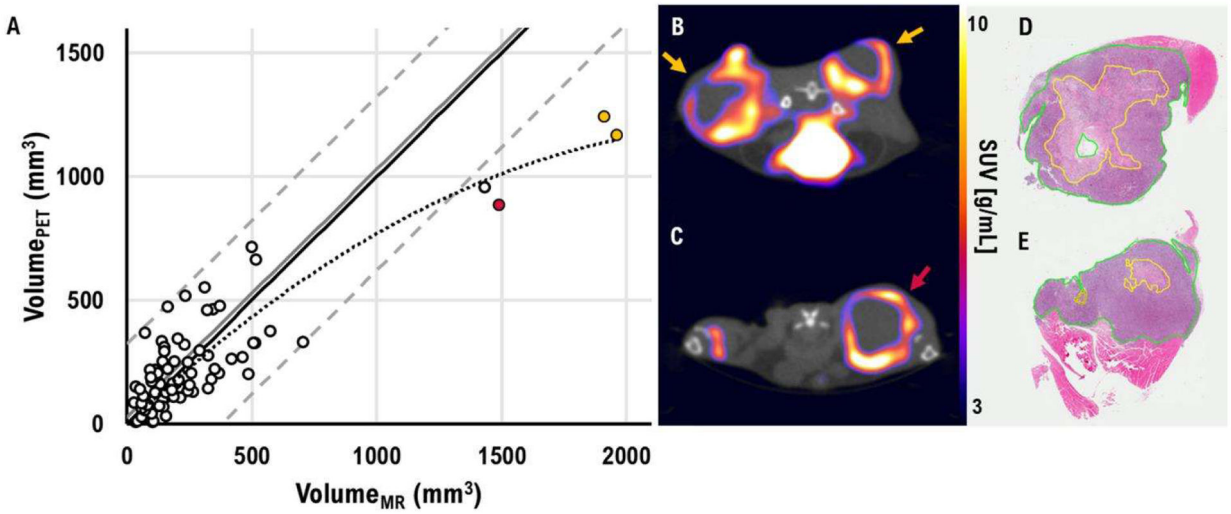

Figure 5.

(A) A scatter plot of tumor volume measured by MR and [^{18}F]FDG PET/CT. The solid black line represents the identity line. The solid gray line indicates the bias of measured volume. The dashed gray line represents 95% confidence interval levels. The dotted gray line represents trend line of tumor volume measured by MR and [^{18}F]FDG PET/CT. The color-coded points represent the measured volumes of the tumors in figure 5B–C. (B-C) An example of an axial [^{18}F]FDG PET/CT image with hypoxic cores. Each color-coded arrow represents the corresponding-colored points in figure 5A. (D-E) A digital histopathological image of the tumor from figure 5B. The solid yellow line represents necrotic cells.

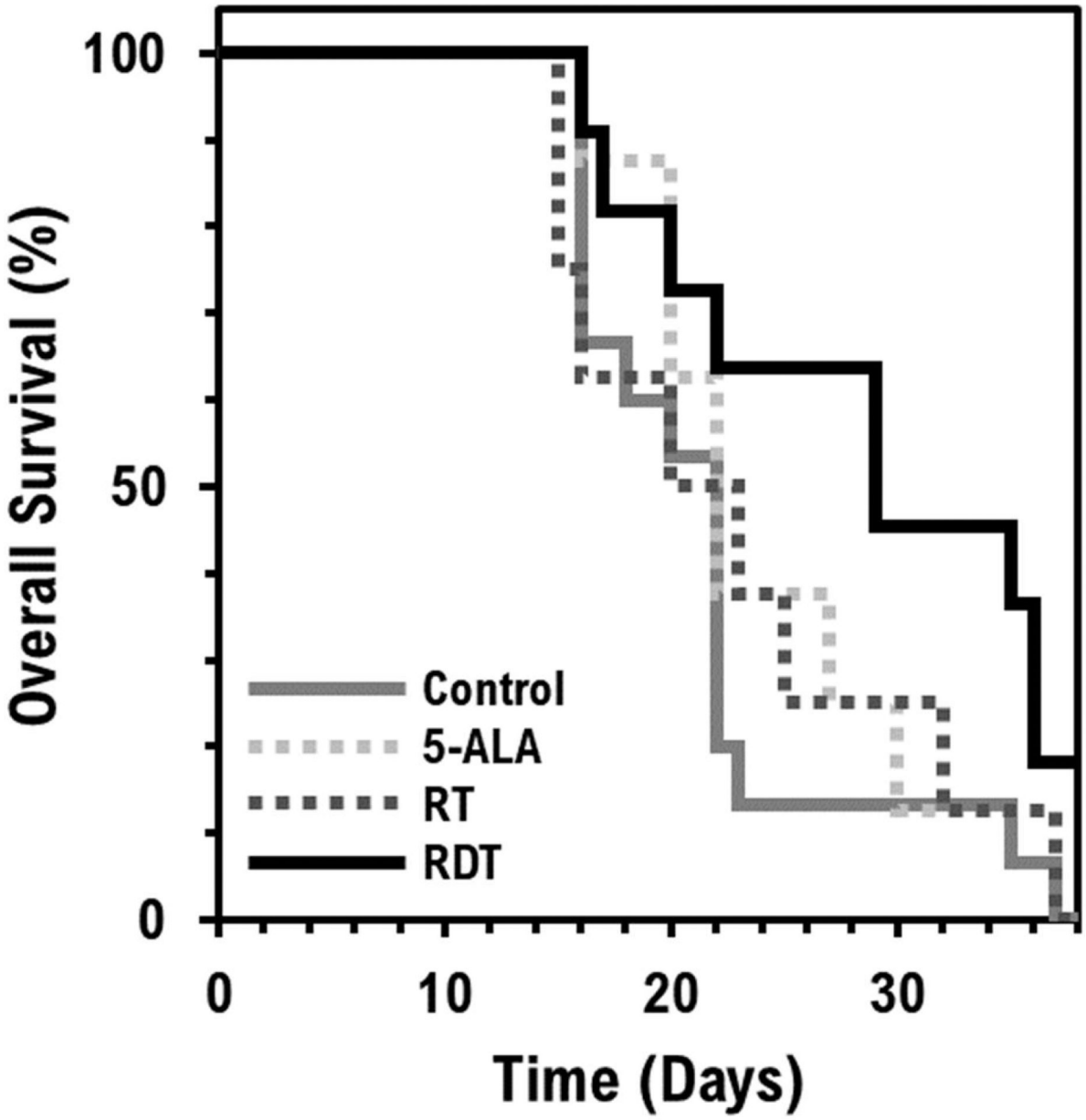

Figure 6.

Overall animal survival. A Kaplan-Meier estimator for RDT treatment is shown in a solid black line and estimators for control, 5-ALA only, and RT only treatment are shown in solid gray, dotted light gray, and dotted dark gray lines, respectively.

Table 1.

A total number of metastases observed in [^{18}F]FDG PET/CT since pre-treatment.

	Number of Metastases*			
Groups	**Pre-treatment**	**3 days post-treatment**	**7 days post-treatment**	**10 days post-treatment**
Control	0	4	9	16
RDT (5-ALA + RT)	0	2	4	6

*A total number of metastatic sites measured in each group